Proceedings of the 5th International Conference of Fluid Flow, Heat and Mass Transfer (FFHMT'18)
Niagara Falls, Canada – June 7 – 9, 2018
Paper No. 175
DOI: 10.11159/ffhmt18.175

Role of Curvature on Heat Flow Visualization and Irreversibilities during Natural Convection in Enclosures

Damodara Priyanka, Tanmay Basak
Department of Chemical Engineering, Indian Institute of Technology Madras
Chennai, India
damodarapriyanka@gmail.com; tanmay@iitm.ac.in

Abstract **-** This article presents a detail analysis of heatlines and entropy generation during natural convection in various enclosures with curve (concave and convex) walls. The dimensions of enclosures are fixed in such a way that thedimensionless area of the cavity is one and the dimensionless length of the wall is one. Two heating strategies are considered such as (a) type 1: hot bottom wall, cold side walls in the presence of adiabatic top wall and (b)type 2: hot left, cold top and bottom walls in the presence of adiabatic right wall. Numerical simulations have been carried out for fluid with Prandtl number Pr = 0. 7 at different Rayleigh number $(10^3 \leq Ra \leq 10^5)$. The distributions of isotherms, streamlines, heatlines and entropy generation due to heat transfer and fluid friction are compared for curved walled enclosures with those of square enclosure. The effect of Ra on the total entropy generation, average Bejan number and average Nusselt number is illustrated for considered enclosures involving both the heating strategies. The optimal configuration and optimal heating strategy is chosen based on the less entropy generation rate and higher heat transfer rate.

Keywords**:** Entropy Generation, Fluid Media, Curved Wall, Natural Convection, Heatline; Concave, Convex.

1. Introduction

Natural convection in curved wall cavities has acquired many researcher's attention due to its significant practical applications. Based on the applicability in various industrial applications, the present study provides comparison of flow and thermal characteristics of fluid within curved (concave/convex) walled enclosures to that of square cavity with same unit area. Further, the comparison is carried out for two heating strategies (Case 1: hot bottom wall, Case 2: Hot left wall, see Figs. 1) via heatline and entropy generation analysis at Pr = 0:7 for wide range of Ra ($10^3 \leq Ra \leq 10^5$). Thus, the comparative study helps to choose proper thermal boundary conditions to achieve higher heat transfer rates and lower entropy generation. And such boundary conditions may be used in designing various heat transfer applications such as solar collectors [1], heat exchangers [2], fuel cells [3] etc.

2. Mathematical Modeling and Simulations

The three dimensional physical domains are represented in the Fig. 1 i(a-c) and ii(a-c). And the computational domains based on semi-infinite approximation along Z direction are shown in the same Fig. 1i(d-f) and ii(d-f). The flow and thermal characteristics are studied based two different cases as follows: Case1: Hot bottom wall, cold side walls and adiabatic top wall [Fig 1(i)]. Case 1: Hot left wall, cold top and bottom walls and adiabatic right wall [Fig 1(ii)]. The square enclosure is modified into two types of curved enclosures concave and convex. The equal area for the three enclosures is achieved by adjusting the length and width of curvature. The computational domain considered in the present study is based on semi-infinite approximation along the Z direction. The fluid assumed to be incompressible and Newtonian. Except density, the thermo-physical quantities of fluid are assumed to be constant. The flow and temperature field is two dimensional, laminar and steady state. The thermal radiation and viscous dissipation effects are sufficiently small to be ignored. Under these assumptions, governing equations for natural convection in terms of conservation of mass, momentum and energy can be written with following dimensionless variables.

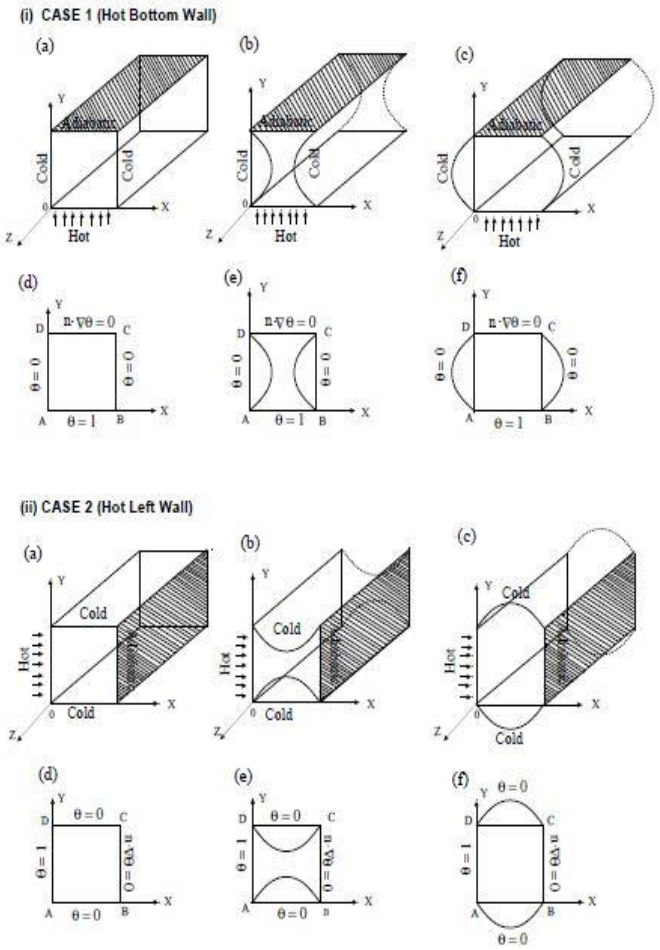

Fig. 1: Schematic diagram of the physical domain of case 1(hot bottom wall, cold side walls and adiabatic top wall a): (i) (a-c) and case 2(hot left wall, cold top and bottom walls and adiabatic right wall): (ii)(a-c) and computational domain of case 1: (i) (d-e) case 2: (ii)(d-e) for square (a, d), concave (b, e) and convex cavities (c, f).

$$\frac{\partial U}{\partial \mathrm{X}} + \frac{\partial V}{\partial Y} = 0 \tag{1}$$

$$U\frac{\partial U}{\partial \mathrm{X}} + \mathrm{V}\frac{\partial \mathrm{U}}{\partial Y} = -\frac{\partial P}{\partial \mathrm{X}} + Pr\left(\frac{\partial^2 U}{\partial X^2} + \frac{\partial^2 V}{\partial Y^2}\right) \tag{2}$$

$$U\frac{\partial \mathrm{V}}{\partial \mathrm{X}} + \mathrm{V}\frac{\partial \mathrm{V}}{\partial Y} = -\frac{\partial P}{\partial \mathrm{Y}} + Pr\left(\frac{\partial^2 U}{\partial X^2} + \frac{\partial^2 V}{\partial Y^2}\right) + RaPr\theta \tag{3}$$

$$U\frac{\partial \theta}{\partial \mathrm{X}} + \mathrm{V}\frac{\partial \theta}{\partial Y} = \frac{\partial^2 \theta}{\partial X^2} + \frac{\partial^2 \theta}{\partial Y^2} \tag{4}$$

and the governing equations [Eqs. ((2)) - ((4))] are subjected to two types of thermal boundary conditions:

(a) Case 1: $U = V = 0$, $\theta = 1$ on wall AB, U =V=0, $\frac{\partial \theta}{\partial Y} = 0$ on wall CD, $U = V = 0$, $\theta = 0$ on walls BC and DA

(b) Case 2: $U = V = 0$, $\theta = 0$ on walls AB and CD, U =V=0, $\frac{\partial \theta}{\partial Y} = 0$ on wall BC, $U = V = 0$, $\theta = 1$ on wall DA

2.1. Streamlines, Heatlines, Nusselt Number and Entropy Generation

The visualization of fluid flow is studied by the streamlines which are mathematically represented streamfunctions (ψ). The relationship between streamfunctions (ψ) and velocity components (U and V) are given as follows:

$$U = \frac{\partial \psi}{\partial Y}, \quad \mathrm{V} = -\frac{\partial \psi}{\partial \mathrm{X}} = 0 \tag{5}$$

which yield a single equation

$$\frac{\partial^2 \psi}{\partial X^2} + \frac{\partial^2 \psi}{\partial Y^2} = \frac{\partial U}{\partial \mathrm{X}} - \frac{\partial V}{\partial Y} \tag{6}$$

The detailed solution procedure is given in the earlier work [4].

A generalized definition on heat transfer coefficient in terms of the local Nusselt number (Nu_s) along the isothermal walls for all enclosures is given as:

$$N_u = -\mathbf{n}.\delta_S \left(\frac{\partial \theta}{\partial \mathrm{X}} \boldsymbol{e_x} + \frac{\partial \theta}{\partial \mathrm{Y}} \boldsymbol{e_y} \right) \tag{7}$$

The expression for unit normal vectors are obtained using the methodology mentioned in the work of Roy [5].

The heat flow within the enclosure is displayed using the heatfunction (Π) obtained from conductive heat fluxes ($-\partial\theta/\partial \mathrm{Y}, -\partial\theta/\partial \mathrm{Y}$) as well as convective heat fluxes ($U\theta$, $V\theta$). The heatfunction equation is as follows:

$$\frac{\partial^2 \Pi}{\partial X^2} + \frac{\partial^2 \Pi}{\partial Y^2} = \frac{\partial}{\partial \mathrm{X}}(U\theta) - \frac{\partial V}{\partial Y}(\mathrm{V}\theta) \tag{8}$$

The above equations are solved using Galerkin finite element method and detailed procedure is explained in the earlier work [4].

Entropy generation due to fluid friction (S_ψ) and heat transfer (S_θ) are calculated using following equations

$$S''' = \frac{k}{{T_0}^2}\left[\left(\frac{\partial T}{\partial x}\right)^2 + \left(\frac{\partial T}{\partial y}\right)^2\right] + \frac{\mu}{T_0}\left[2\left(\left(\frac{\partial u}{\partial x}\right)^2 + \left(\frac{\partial u}{\partial y}\right)^2\right) + \left(\frac{\partial u}{\partial x} + \frac{\partial v}{\partial y}\right)\right] \tag{9}$$

The detailed mathematical procedure for solving the above equation are discussed in the earlier works [6].

A dimensionless parameter, Bejan number (Be_{av}) is often used to understand the relative dominance of fluid friction and heat transfer irreversibilities via following relationship:

$$Be_{av} = \frac{S_{\theta,total}}{S_{\theta,total} + S_{\psi,total}} = \frac{S_{\theta,total}}{S_{total}} \tag{10}$$

In agreement with the above definition, Be_{av}>0.5 signifies the dominance of heat transfer irreversibility and Be_{av}<0.5 signifies the dominance of fluid friction irreversibility.

3. Results and Discussion

The numerical simulations are carried out in terms of streamlines (ψ), isotherms (θ), heatlines (Π), entropy generation due to fluid friction (S_ψ) and entropy generation due to heat transfer (S_θ) for Pr= 0.7 at Ra = 10^3-10^5 for 28×28 bi-quadratic elements. At the low Ra the magnitude of streamfunction is lower resulting in the dominance of the conduction heat

transfer and heatlines are orthogonal to the isothermal walls in all the enclosures (Figures are not shown). At higher *Ra* ($Ra = 10^5$), due to high velocity gradients, higher intensities of fluid rotation cells are observed

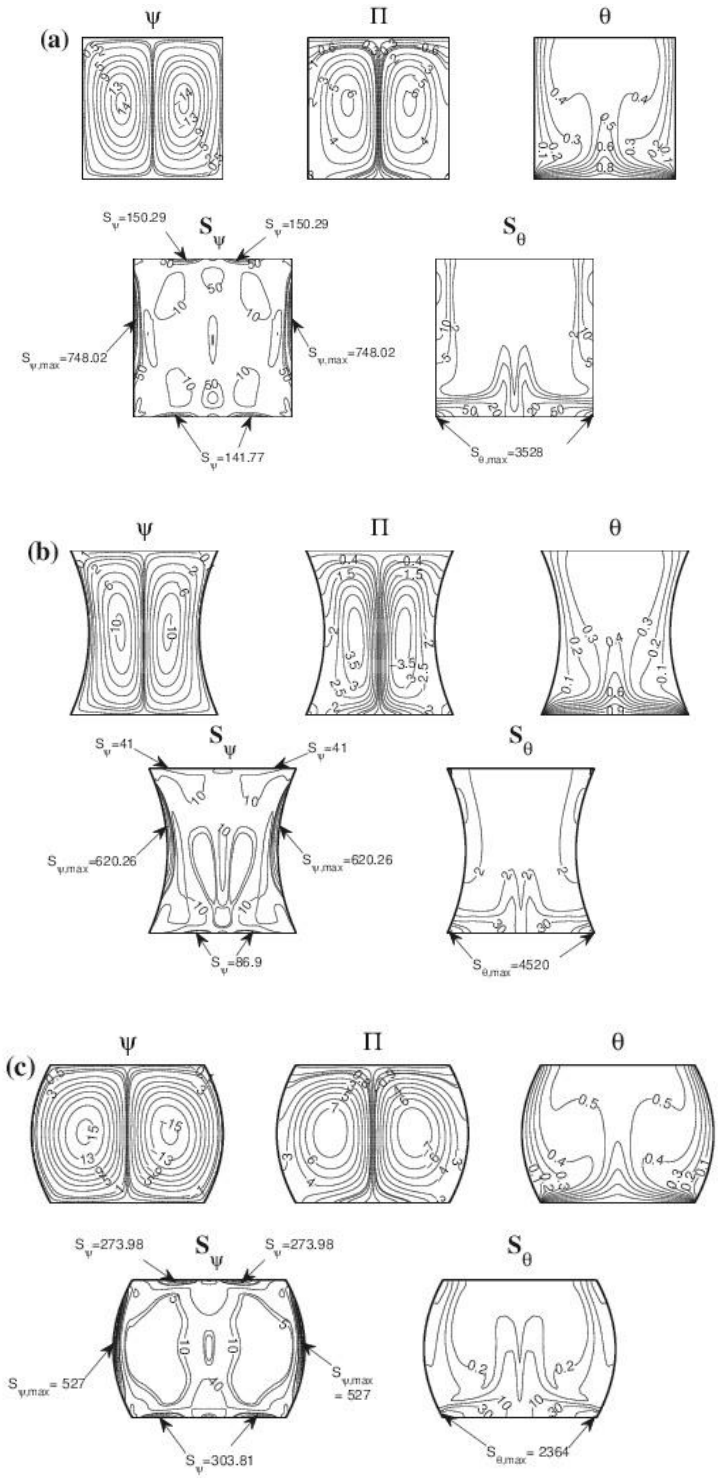

Fig. 2: Streamlines (ψ), heatlines (Π), isotherms (θ), local entropy generation due to heat transfer (S_θ) and loca entropy generation due to fluid friction (S_ψ) within (a) square(b) concave and (c) convex cavities with unit area, with isothermal hot bottom wall, cold side walls and adiabatic top wall at $Pr = 0.7$, $Ra = 10^5$.

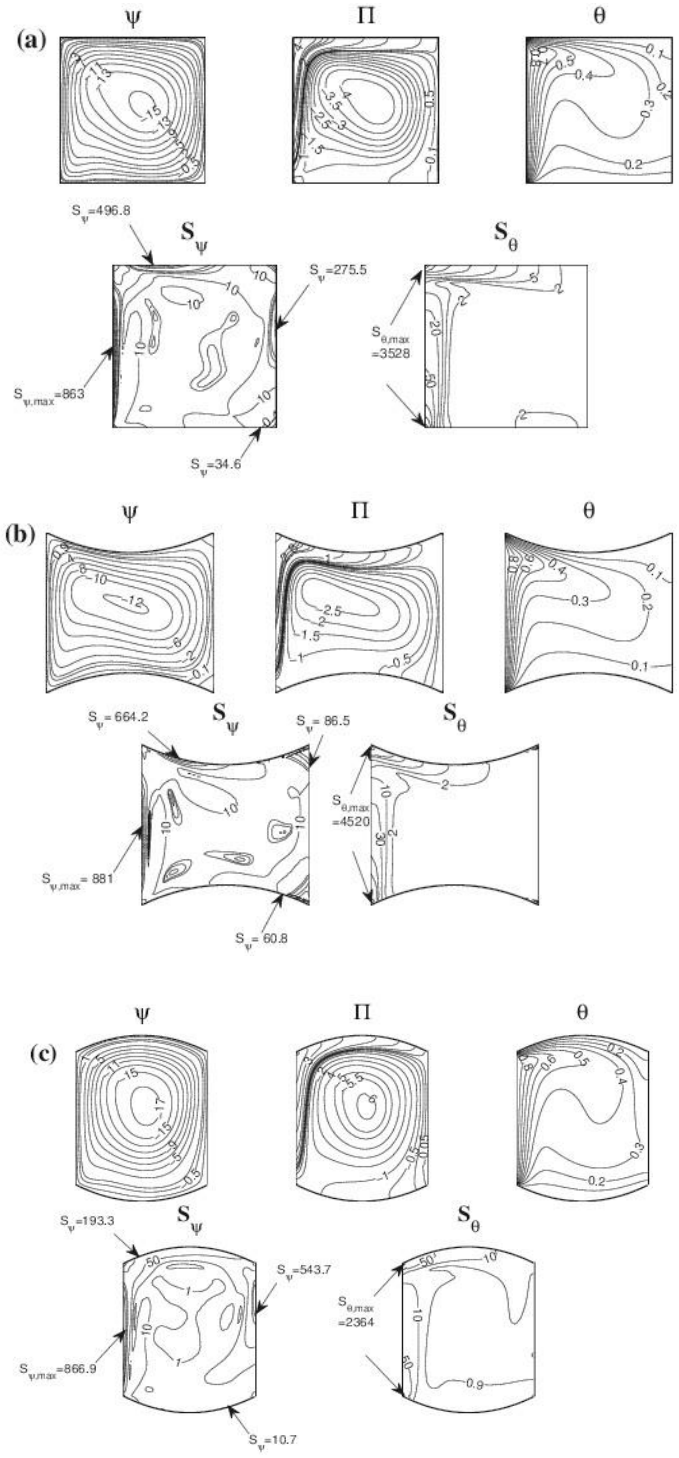

Fig. 3: Streamlines (ψ), heatlines (Π), isotherms (θ), local entropy generation due to heat transfer (S_θ) and loca entropy generation due to fluid friction (S_ψ) within (a) square(b) concave and (c) convex cavities with unit area, with isothermal hot left wall, cold top and bottom walls and adiabatic right wall at $Pr = 0.7$, $Ra = 10^5$.

denoting convective dominant regime in all the enclosures. Fluid rises up from the hot wall due to buoyancy force and cools down based on the presence of the cold walls in both the cases (case 1:(Fig. 2(a-c)) and case 2: Figs. 3 (a-c))). Due to

symmetric boundary conditions of case 1 enclosures, the clockwise and anticlockwise streamline cells are seen near the left and right halves, respectively involving all the enclosures (Figs. 2(a-c))). Common to both the cases, convex cavity corresponds (Figs. (2-3)(c)) to higher values of streamfunction as distance between the cold wall is higher compared to the square and concave enclosures. However, case 2 enclosures exhibit comparatively higher streamfunction magnitudes than those of case 1. Common to both the cases, complicated end-to-end and closed loop heatlines are observed in all the three cavities. The presence of circular closed loop heatlines depicts the dominance of convective heat transfer. On the other hand, the heatlines at the hot-cold junction (left and right bottom corners for case 1 and top and bottom corners of left wall for case 2) are perpendicular to isotherms depicting conduction heat transfer. The isotherms at the core are highly curved signifying the convective effect. The maximum temperature gradients are noted at the at hot-cold junctions. Due to larger velocity gradients, larger values of S_{ψ} are observed in both case 1 and case 2. However, case 2 (Figs. 3) enclosures exhibits larger S_{ψ} values than those of case 1 (Figs. 2). The highest values of entropy generation due to fluid friction ($S_{\theta,max}$ = 4520, 3528 and 2364 for concave, square and convex respectively) is observed at the hot cold junctions due to larger temperature gradients. Common to all enclosures, S_{θ} is observed to be significantly low at the other portions (expect at the hot cold junctions) of all the cavities.

Figs. 4(a-b) demonstrate the variations of S_{total}, Be_{av}, $\overline{Nu_b}$for case 1 and $\overline{Nu_l}$ for case 2 with Ra involving square, concave and convex enclosures at Pr=0.7. As the contribution of $S_{\psi,total}$ to the total entropy generation (S_{total}) is negligible within $10^3 \leq Ra \leq 10^4$ in all the cavities, S_{total} is contributed mainly due to $S_{\theta,total}$. Consequently, the increase of S_{total} with Ra is insignificant for $Ra \leq 10^4$ (Figs. 4(a-b) (i)). However, velocity gradients increase beyond $Ra = 10^4$ resulting in significant increase n $S_{\psi,total}$. Therefore, common to all enclosures, a rapid increase in S_{total} is observed. The maximum value of S_{total} occurs at $Ra = 10^5$. At $Pr = 0.7$, irrespective of the geometry of the enclosures, the total entropy generation (S_{total}) is significantly larger in case 1 compared to case 2 throughout the range of Ra. The distribution of Bejan's number (Be_{av}) explains the relative dominance of heat transfer and fluid friction irreversibilities (see Figs. 4(a-b) (ii)). It is observed that, Be_{av} decreases with Ra irrespective of geometry of the enclosure. At the low Ra, $S_{\theta,total}$ contributes largely to the S_{total} and hence Be_{av} corresponds to the maximum value (Be_{av} = 1) in all the enclosures. Common to all the enclosures, as Ra increases beyond 10^4, the fluid flow irreversibility increases rapidly consequently, Be_{av} also displays a sharp decline (see Fig. 4(a-b) (ii)). As the trend of increment in the values of $S_{\psi,total}$ and $S_{\theta,total}$ with Ra is almost similar in all the three enclosures, the variation of Be_{av} is observed to be similar. As seen from Fig. 4(a-b) (iii), the increase of Nu_b with Ra for the three enclosures is almost invariant with Ra till $Ra \leq 10^4$ especially in the case 1 enclosures as the exergy loss due to irreversibilities does not influence significantly the heat transfer rate due to thermal gradients ($\overline{Nu_b}$), thereafter Nu_b increases gradually with Ra. As Ra increases to 10^5, the intense convective effect results in higher heat transfer rates and thus $\overline{Nu_b}$ attains maximum value at $Ra = 10^5$ in all the enclosures. The heat transfer rates are higher in the concave cavity in the entire range of Ra compared to the square and convex (enclosures in both the cases (see Fig. 4(a-b) (iii)). This may be due to the higher thermal gradients due to the least distance from the cold curved walls of the concave cavity in both the cases. Overall, concave cavity may be optimal based on the higher heat transfer rates with similar order of entropy generation for all geometries (see Figs. 4(a-b)).

4. Conclusion

The present work provides a detailed analysis to identify a thermally efficient enclosure among the curved wall cavities (convex and concave) and compare the performance with a regular square enclosure corresponds to equal area (unit area) via heatline and entropy generation based analysis at the low and high Ra for Pr = 0.7.The comparative study of three different geometries show that the heat and fluid flow distributions are found to be significantly affected by the height of the enclosure and the curvature of the walls. Further, the comparative study helps to choose proper thermal boundary conditions to achieve higher heat transfer rates and lesser entropy generations. Common to both the cases among the three enclosures, the concave enclosure is preferred over the square and convex enclosure as the concave enclosure is corresponds to comparatively higher heat transfer rates and almost similar entropy generation rates. On the other hand, heat flow visualization and heatline analysis states that, convex enclosure lead to enhanced flow intensities and thermal mixing. Although case 1 enclosures correspond to slightly higher heat transfer rates based on the lower entropy generation, the case 2 boundary conditions are considered as the optimal heating strategy for the efficient heat transfer rate and reduced irreversibilities (less entropy generation or exergy loss) for all Ra at Pr = 0.7.

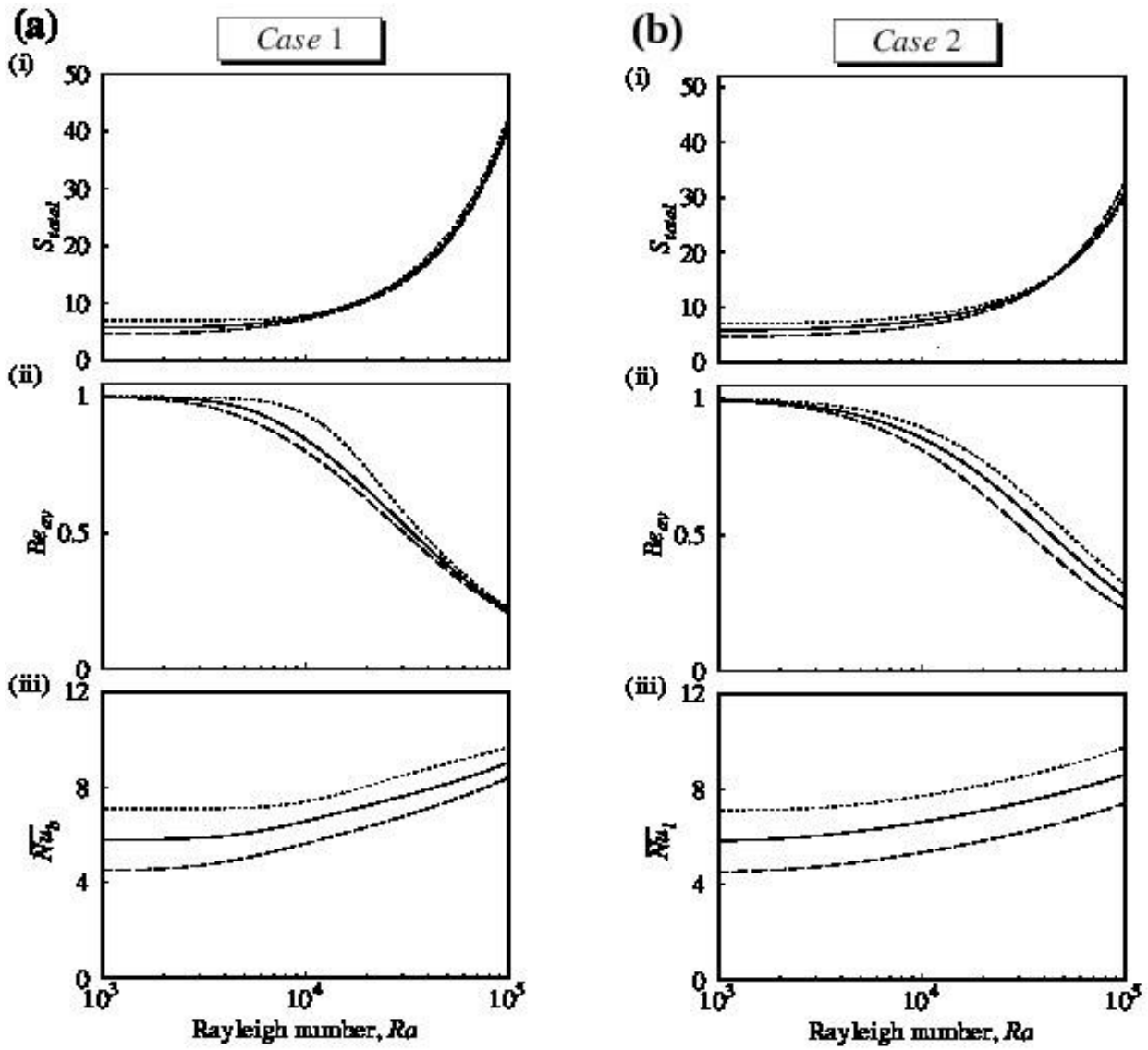

Fig. 4: Variation of the total entropy generation(S_{total}:(a-b)i), average Bejan number(Be_{av}:(a-b)ii) and the average Nusselt number alone hot bottom wall($\overline{Nu}_b$:(a iii)) and hot left wall ($\overline{Nu}_l$:(b iii)) with *Ra* for both case 1 and cass 2 [square(—),concave(_ _ _) and convex(- - -)] cavities at Pr=0.7.

Nomenclature

Be	Bejan number
f	function
g	acceleration due to gravity, m s^{-2}
k	thermal conductivity, W m^{-1} K^{-1}
N	total number of nodes
n	normal vector to the plane
Nu	*local* Nusselt number
$\overline{Nu}$	average Nusselt number
p	pressure, Pa
P	dimensionless pressure

Ra Rayleigh number
S dimensionless entropy generation
S_θ, S_ψ dimensionless entropy generation due to heat transfer and fluid friction, respectively
S_{total} dimensionless total entropy generation due to heat transfer and fluid friction
T temperature, K
u, v x and y components of velocity, respectively m s^{-1}
U, V X and Y components of dimensionless velocity, respectively
X, Y dimensionless distances along x and y coordinate, respectively

Greek symbols

α thermal diffusivity, $m^2 s^{-1}$
β volume expansion coefficient, K^{-1}
γ penalty parameter
$\boldsymbol{\theta}$ dimensionless temperature
ν kinematic viscosity, $m^2 s^{-1}$
ρ density, kg m^{-3}
Φ basis functions
Π dimensionless heatfunction
ψ streamfunction
Ω two dimensional domain

Subscripts

b bottom wall *l* left wall *r* right wall *t* top wall

Reference

[1] F. Suarez, S. Tyler and A. Childress, "A fully coupled, transient double-diffusive convective model for salt-gradient solar ponds," *Int. J. Heat Mass Tran,* vol. 43, pp. 1718-1730, 2010.

[2] A. Carotenuto and C. Casarosa, "A lumped parameter model of the operating limits of one-well geothermal plant with down hole heat exchangers," *Int. J. Heat Mass Tran,* vol. 43, pp. 2931-2948, 2000.

[3] J. K. Kuo and C. K. Chen, "The effects of buoyancy on the performance of a pem fuel cell with a wavelike gas flow channel design by numerical investigation," *Int. J. Heat Mass Tran,* vol. 5, pp. 4166–4179, 2007.

[4] T. Basak and S. Roy, "Role of 'bejan's heatlines' in heat flow visualization and optimal thermal mixing for differentially heated square enclosures," *Int. J Heat Mass Transfer,* vol. 51, pp. 3486–3503, 2008.

[5] M. Roy, P. Biswal, and T. Basak, "On the finite element based evaluation of nusselt numbers for curved walls," *Int. Comm. Heat Mass Tran,* vol. 77, pp. 123-131, 2016.

[6] T. Basak, R. Anandalakshmi, S. Roy and I. Pop, "Role of entropy generation on thermal management due to thermal convection in porous trapezoidal enclosures with isothermal and non-isothermal heating of wall," *Int. J Heat Mass Tran,* vol. 67, pp. 810-828, 2013.